



Lawrence Berkeley Laboratory

UNIVERSITY OF CALIFORNIA

Presented at the Colloque Franco-Japonais de Physique
Nucleaire avec des Ions Lourds, Saclay, France,
October 8-12, 1979

COMPLEX FRAGMENT EMISSION IN RELATIVISTIC HEAVY ION COLLISIONS

M. -C. Lemaire

October 1979

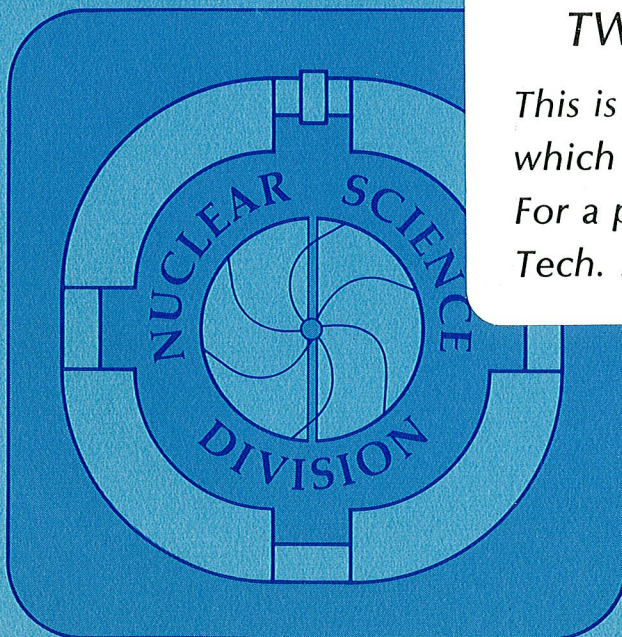
RECEIVED
LAWRENCE
BERKELEY LABORATORY

APR 11 1980

LIBRARY AND
DOCUMENTS SECTION

TWO-WEEK LOAN COPY

*This is a Library Circulating Copy
which may be borrowed for two weeks.
For a personal retention copy, call
Tech. Info. Division, Ext. 6782.*



COMPLEX FRAGMENT EMISSION IN RELATIVISTIC HEAVY ION COLLISIONS

M.-C. LEMAIRE

DPh-N/ME, CEN Saclay, BP 2, 91190 Gif-sur-Yvette, France

Lawrence Berkeley Laboratory, University of California
Berkeley, California 94720

Data relative to proton and pion production produced in central collisions have been reviewed by S. Nagamiya (1). Therefore, the present talk deals mainly with the production of complex fragments. The first section will be devoted to a presentation of experimental data on d, t, ^3He emission and their discussion in terms of the existing models. The size of fireball derived from the analysis of complex fragments will be compared to the results of pion interferometry experiment in section II. Interesting features observed in the distribution of charged particles once an heavy fragment has been detected will be reported in section III. Finally, suggestions of phenomena to study with a 4π detector will be given in section IV.

I. EMISSION OF LIGHT FRAGMENTS

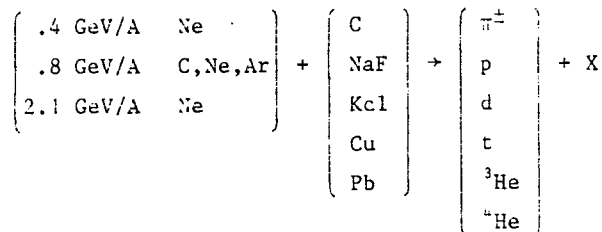
From streamer chamber pictures or emulsion data, it is known that central collisions are violent processes which produce events with fairly large transverse momenta and high multiplicities. Therefore, Nagamiya's experiment (2,3) has been devoted to measure light fragments in a kinematic region corresponding to high transverse momenta and intermediate rapidities. Both inclusive data and spectra biased on high multiplicity have been recorded. The systems which have been studied are listed in Table I. Comparing Nagamiya's experiment to Poskanzer-Gutbrod's experiment (4,5,6) the first one was oriented to the measurement of more energetic fragments than in the second one, so that events of higher transverse momenta have been studied.

A. Experimental data

Momentum spectra of protons, deuterons and tritons expressed in units of GeV/c/nucleon are displayed on Fig. 1 for the C + C system. All these momentum spectra are smoothed in contrast to those observed in a fragmentation type process as these latter exhibit a peak for fragments produced with the beam

Table 1

Systems studied in the E299H experiment



Range in energy of the detected particles

S. Nagamiya et al.(1-3) Poskanzer-Gutbrod et al.(4-6)

Pions	30 - 900 MeV	17 - 100 MeV
Protons	50 - 2200 MeV	5 - 200 MeV
Deutons	50 - 1300 MeV/A	3 - 125 MeV/A
Tritons	20 - 700 MeV/A	2 - 100 MeV/A
Helium-3	80 - 700 MeV/A	30 - 100 MeV/A
Helium-4	50 - 450 MeV/A	30 - 110 MeV/A

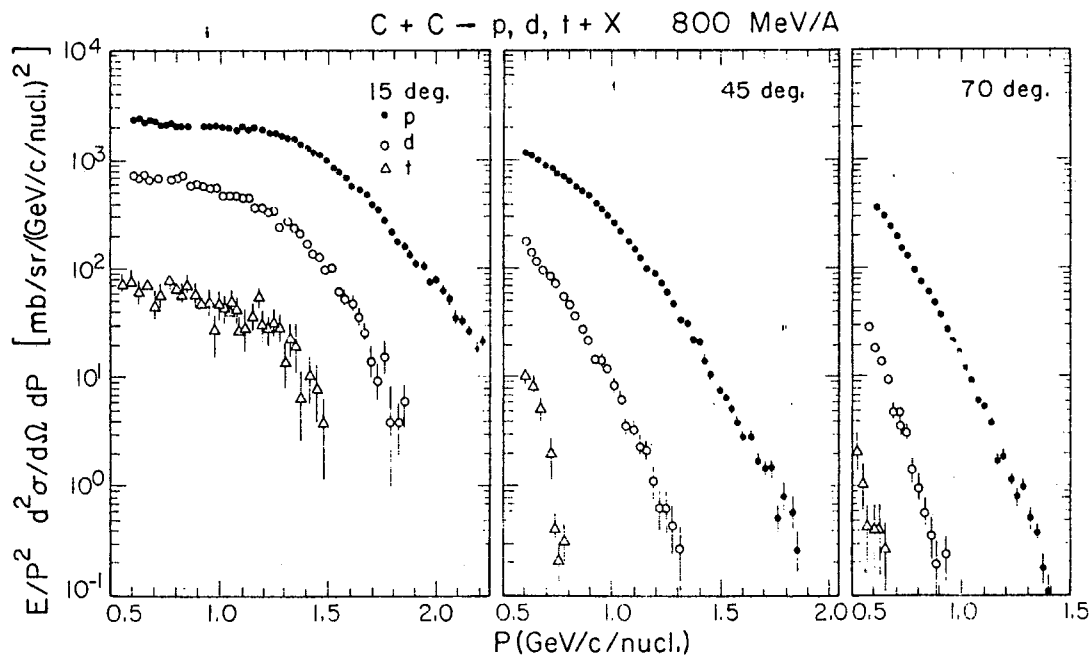


Fig. 1 - Momentum spectra of protons, deuterons and tritons.

velocity (7). At the most forward angles (10-15 degrees) these spectra are quite flat in the low momentum region while the invariant cross-sections decrease exponentially in the high momentum region. For a given fragment, the slope of this high momentum tail becomes steeper when the detection angle increases.

At a given detection angle, it becomes steeper when the mass of the fragment increases. The yield of deuterons and tritons relative to protons is momentum and angle dependent. The largest contribution occurs at forward angles and low momenta. The relative yield of complex fragments to protons increases with the size of the target-projectile combination. Consequently, in some kinematic regions, the charged particle spectra can be quite different from the proton spectra. To investigate further these differences, the ratio R between the charged particle and proton spectra has been calculated as a function of momentum at different detection angles :

$$R = \sum_i Z_i \left(E_i \frac{d^3\sigma_i(p)}{dp^3} \right) / \left(E_P \frac{d^3\sigma_P(p)}{dp^3} \right) \quad (1)$$

where i stands for p , d , t , ${}^3\text{He}$ and ${}^4\text{He}$. The results are displayed on Fig. 2 for few of the systems studied. It shows that for Ar projectile the yield of complex fragments can exceed by a factor 1.5 that of protons in the low momentum region, while for C projectile it never exceeds 40 % of the proton yield.

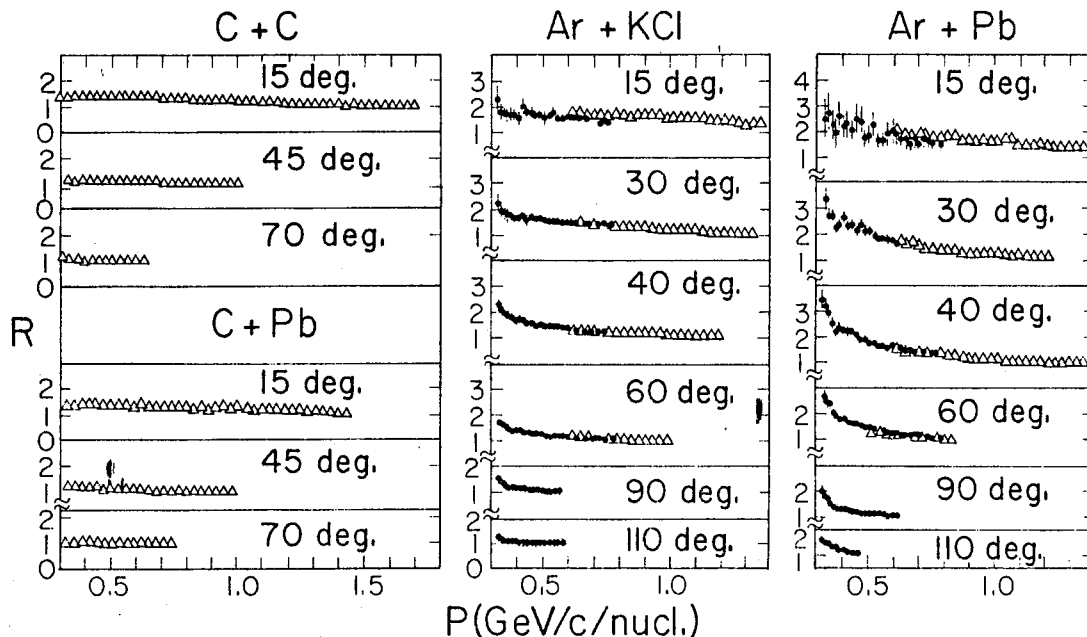


Fig. 2 - Ratio R of the charged particle yield to the proton yield as a function of momentum.

Examples of energy dependence of the deuteron momentum spectra are shown on Fig. 3 for the Ne + Pb and Ne + NaF systems. For Pb target, at 30 degrees, the deuteron cross-section is independent of incident energy for momentum smaller than 1.5 GeV/c (which corresponds to 260 MeV/nucleon kinetic energy). It

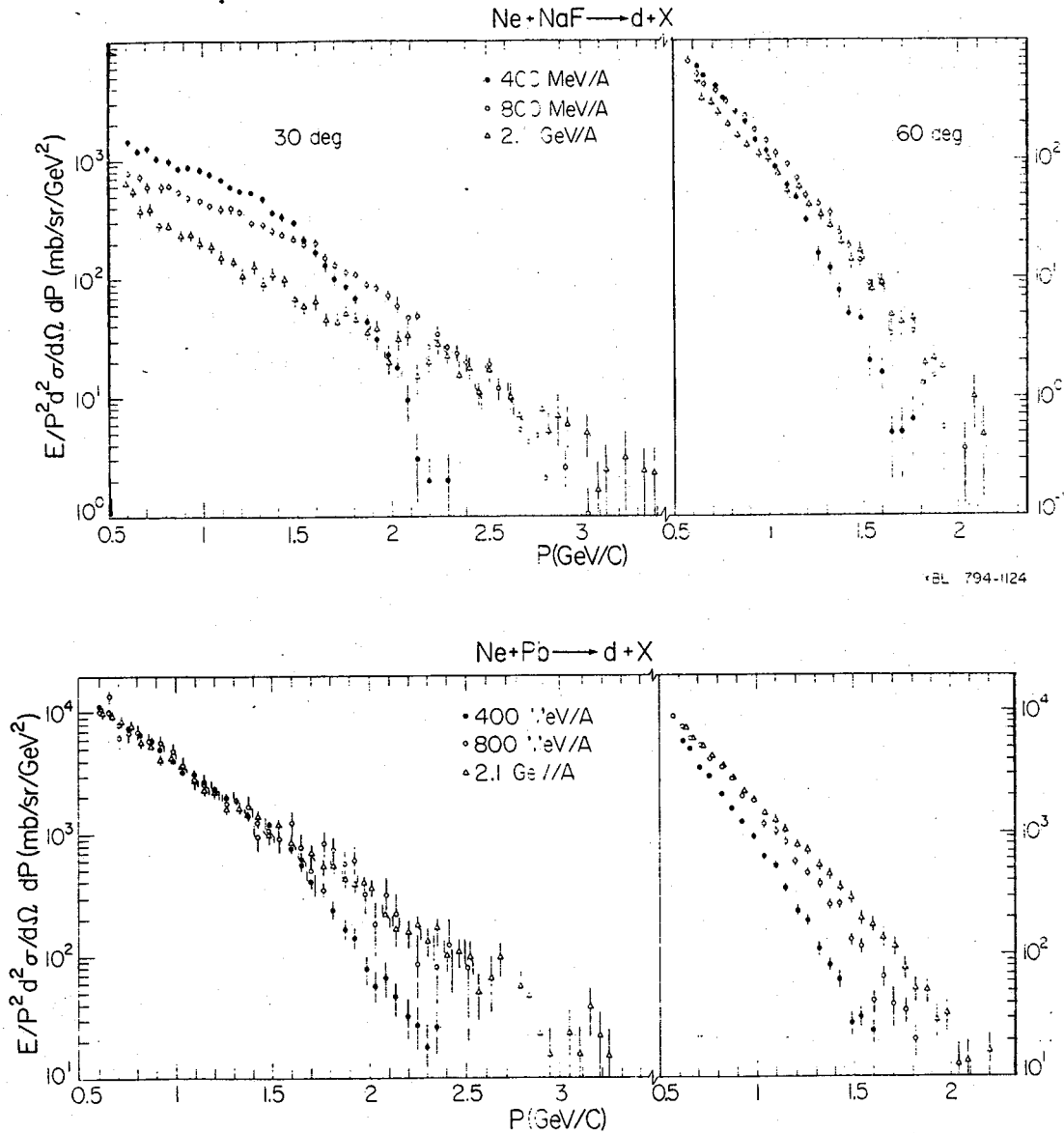


Fig. 3 - Energy dependence of the deuteron momentum spectra.

confirms the observation reported earlier (6) that, in the $^{20}\text{Ne} + ^{238}\text{U}$ system the 30 degrees ^3He energy does not depend on incident energy for kinetic energies of the ^3He smaller than 100 MeV/nucleon. Such a behavior is characteristic of a limiting fragmentation process suggesting that contributions from target spectator fragments are dominant in this kinematic region, at least, for heavy targets (8). In the high momentum tail, the cross-sections decrease more steeply at 400 MeV/A than at the higher incident energies as less kinetic energy is available to produce high momentum fragments when the incident energy is low. At 60 degrees, the slope decreases with increasing bombarding energy. In

case of NaF target, the 30 degrees low momentum cross-section depends on the incident energy suggesting that in case of light targets, target spectator fragments do not contribute very much in this kinematic region.

The shapes of the momentum spectra do not depend on the projectile (Fig. 4), there is just a slight increase of the cross-section by a factor of about 1.5 to 2 when the beam changes from ^{20}Ne to ^{40}Ar . Fig. 5 shows the target dependence of the momentum spectra. An increase of the yield is observed when the target becomes heavier. The rate of such increase is strongly momentum dependent and reaches its highest value in the low momentum region.

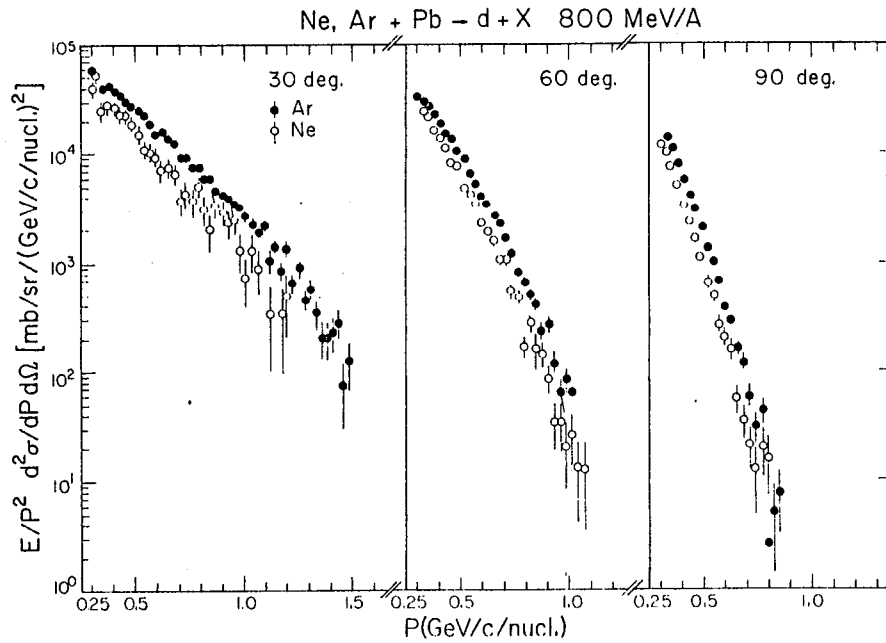


Fig. 4 - Projectile dependence of the deuteron momentum spectra

To visualize the kinematic region to which are associated the present data, contour plots of invariant cross-sections have been plotted in the plane of transverse momentum versus rapidity for the Ar + Pb systems (Fig. 6). A nice feature of such representation is that a transformation from one frame to another is just achieved with a translation on the rapidity axis. The lines join points of same invariant cross-sections. From other experiments, it is well established that projectile and target fragments show up as two mountains at $P_T = 0$ and centered respectively around the projectile and target rapidities. Both the inclusive and high multiplicity data exhibit contributions from target-spectator fragments. This is consistent with the previous observation

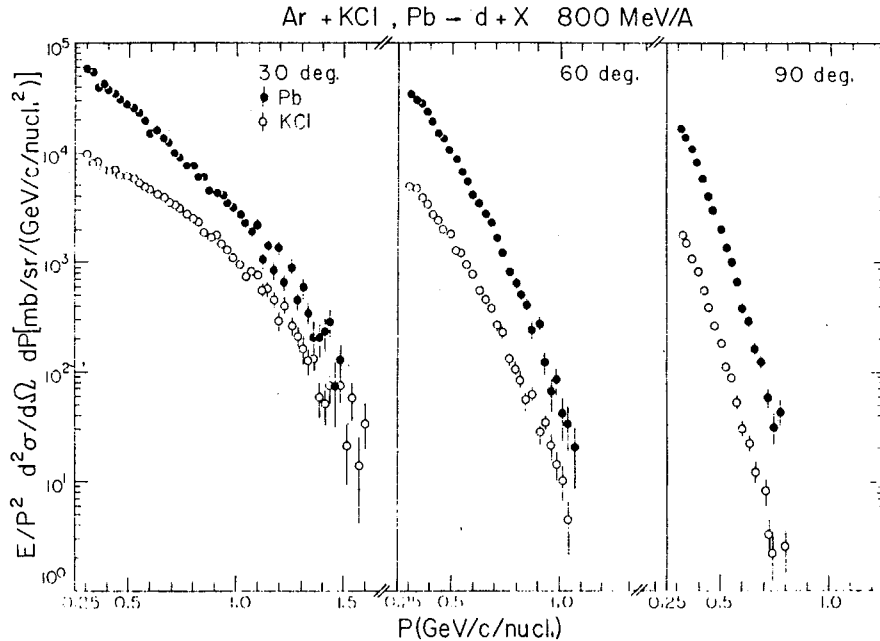


Fig. 5 - Target dependence of the deuteron momentum spectra.

that, at 30 degrees the cross-sections of low momentum fragments are energy independent. In case of symmetric systems like Ar + KCl, the center of mass is well defined. Therefore, the invariant cross-sections have been plotted in the plane of transverse momentum versus parallel momentum calculated in the c.m. frame (Fig. 7). In such representation isotropic emission is characterized by semi-circular contour plots. The experimental cross-sections are forward and backward peaked. This anisotropy is reduced when selection on high multiplicity events is performed. The corresponding center of mass distributions are displayed on Fig. 8. The 90° c.m. spectra are well described by an exponential form $e^{-T_{c.m.}/T}$ with a slope factor T of 108 MeV for the inclusive data and 117 MeV for the high multiplicity data. Such slope is also observed for the low energy protons while the high energy protons have a much steeper slope of $T = 74$ MeV for the inclusive data and $T = 83$ MeV for the high multiplicity data. At 800 MeV/A, the present deuteron spectra do not extend to high energy enough to establish if the high momentum tail will be as steep as for the protons. However, the 400 MeV/A, Ne + NaF data (Fig. 9) suggests that it will occur as the high momentum tail has the same steep slope than the protons ($T = 49$ MeV) while the low momentum deuterons decrease less steeply (T is higher).

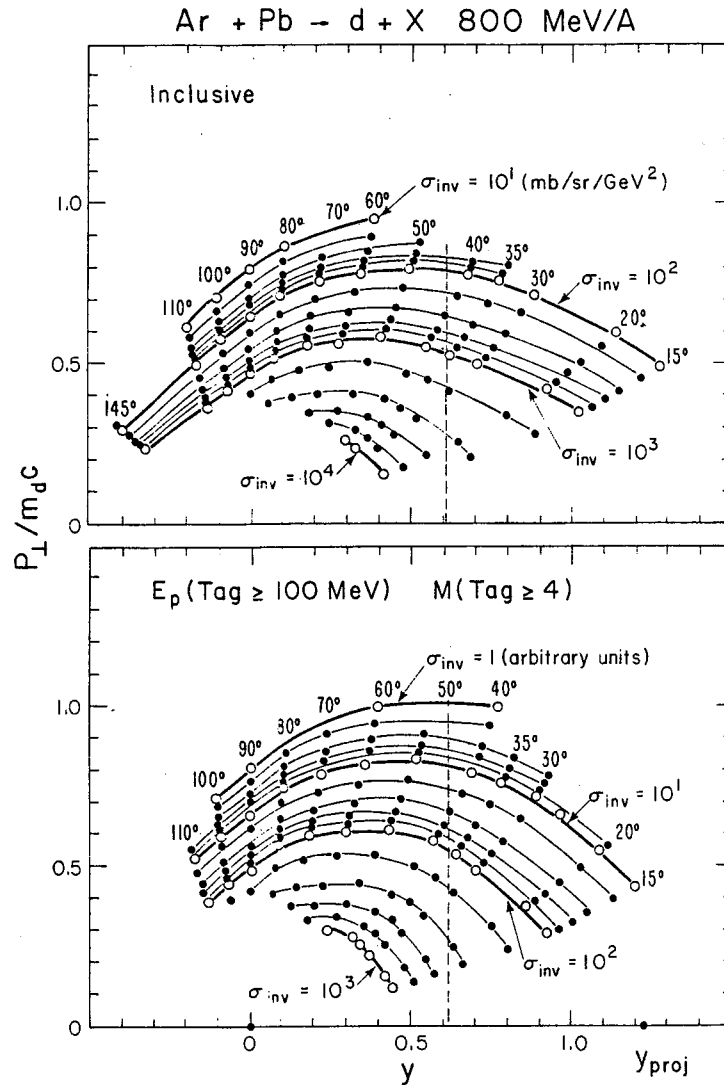


Fig. 6 - Contour plots of invariant cross-sections.

B. Models for complex fragment production

The existing data have been described in terms of various models : coalescence (5,6), thermal (9-10) and firestreak models (11). The first description of composite particle production was via final state interaction or coalescence of the emitted nucleons. In this model, nucleons which have relative momenta less than a coalescence radius P_0 will coalesce to produce a composite particle. It predicts that the cross-sections for the emission of light nuclei of mass A are simply related to the A^{th} power of the cross-section for the emission of nucleons at the same momentum per nucleon :

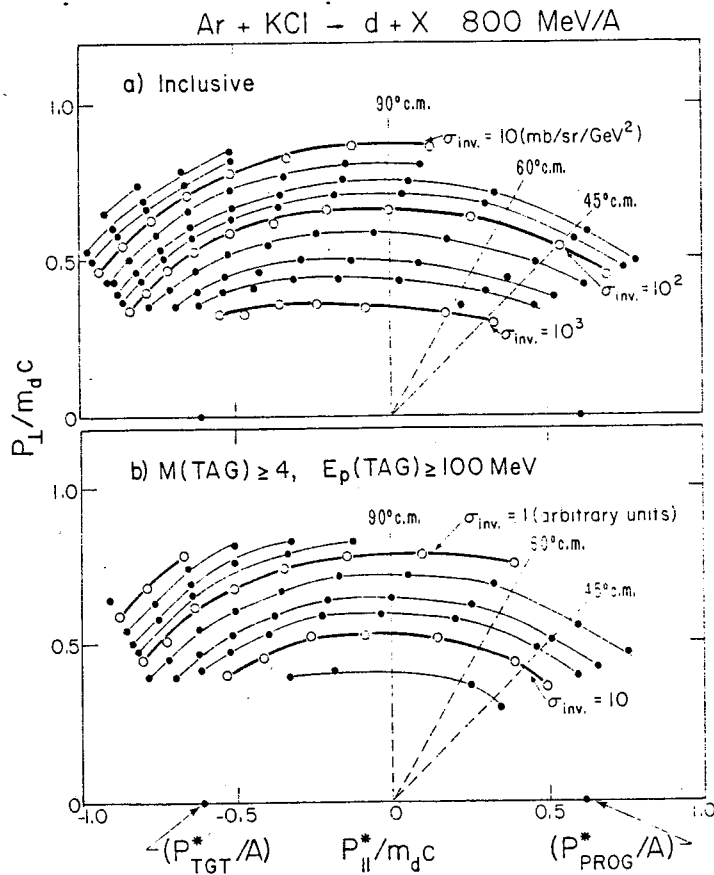


Fig. 7 - Contour plots of invariant cross-sections

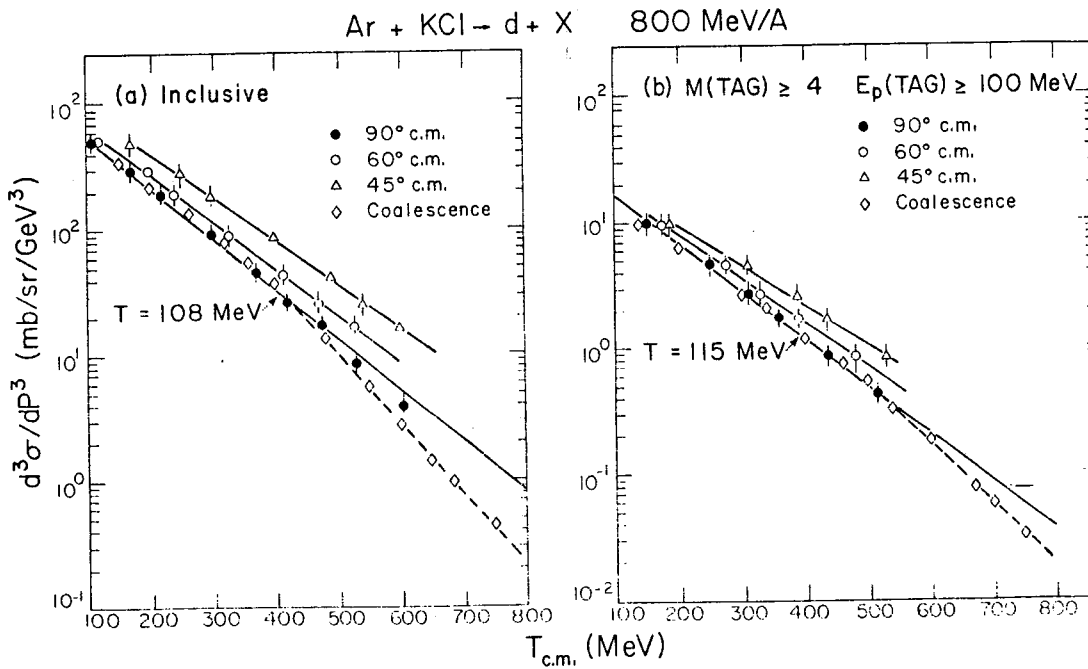


Fig. 8 - Center of mass kinetic energy distributions

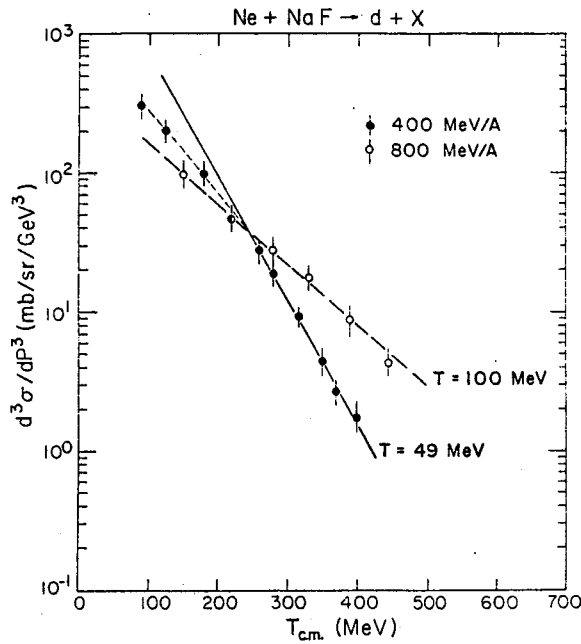


Fig. 9 - Deuteron spectra at $\theta_{c.m.} = 90^\circ$ in Ne + NaF collision at 400 and 800 MeV/A incident energies.

$$E_A \frac{d^3 \sigma_A}{dp_A^3} = C \left(E_P \frac{d^3 \sigma_P}{dp_P^3} \right)^A \quad (2)$$

where $p_A = A \cdot p_P$ and C is a constant independent of the momentum of the particle and of the detection angle. The coalescence radius p_0 is related to this constant C by :

$$p_0^3 = \frac{3 m \sigma_0}{4\pi} x!y! \left[\frac{Z_P + Z_T}{N_P + N_T} \right]^y (x+y)^2 C^{\frac{1}{x+y-1}} \quad (3)$$

where x and y are respectively the proton and neutron numbers in the composite particle ($A = x+y$), Z_P and N_P are the proton and neutron numbers in the projectile, Z_T and N_T are the proton and neutron numbers in the target, σ_0 is the nucleus-nucleus total reaction cross-section and m is the nucleon mass. It has been shown (5,6) that such model reproduces well the energy spectra of the complex fragments for laboratory energies smaller than 100 MeV/nucleon with a p_0 value of about 130 MeV/c. It was therefore interesting to investigate if the relationship given by eq.(2) was satisfied in a much wider kinematic range. In addition, as the normalization of these data are in process of revision (12), the p_0 values are not anymore valid. It is therefore worthwhile to derive the p_0 values from independent experimental data. While the coalescence model does not make any assumption on the mechanism of nucleon production, the relationship given by eq.(2) is also predicted by thermal models (9,10). There, it is assumed that the nucleons of the overlap region form a fireball which expands to a size and density where the collisions between, its constituents become negligible. Therefore, the emitted fragments reflect the properties of the fireball at the point where the interactions stop for which we have the "freeze-out" or "break-up" density. The light fragments can then be produced

either via chemical equilibrium inside the fireball (9) or by coalescence of the nucleons at the end of the fireball expansion (10). An interesting feature of the thermal model of ref.(9) is that there is an explicit reference to the volume V of the fireball in the equation which relates the cross-section for production of a particle of mass A to the A^{th} power of the proton cross-section

$$\frac{d^3N_o(x,y)}{dp^3} = \frac{A^3}{2^A} z_{\text{int}}(x,y) \left(\frac{h^3}{V}\right)^{A-1} R^N \left(\frac{d^3N_n}{dp_n^3}\right)^A \quad (4)$$

where R is the ratio of neutron to proton number for the combined target projectile system ; $z_{\text{int}}(x,y)$ is the internal partition function of the composite

$$z_{\text{int}}(x,y) = \left[\sum_j (2S_j+1) e^{-E_j/T} \right] e^{|E_o|/T} \quad (5)$$

The sum is running over the ground and excited states of the composite, S_j is the spin of the state, E_j its excitation energy and E_o is the ground-state binding energy.

Mekjian (9) has shown that the volume V of the fireball can be expressed as a function of the coalescence radius in momentum space \tilde{p}_o as :

$$V = \left[x!y! e^{E_o/T} \right]^{1/A-1} \left(\frac{3 h^3}{4\pi \tilde{p}_o^3} \right) \quad (6)$$

where \tilde{p}_o is derived from p_o by explicitly removing spin alignment and phase factors (9) :

$$(\tilde{p}_o^3)^{A-1} = \frac{2^A}{A^3(2S+1)} (p_o^3)^{A-1} \quad (7)$$

As the temperatures involved in relativistic heavy ion collisions are high, the term $(e^{E_o/T})^{1/A-1}$ can be replaced by 1 with a good approximation and the relationship between V and \tilde{p}_o corresponds simply to what is expected from phase space. With the p_o values derived previously for the Ne + U system at 400 MeV/A, Mekjian (9) found a radius of the fireball of 5 to 7 fm depending on the nature of the emitted composite particle. These large values of the source sizes were consistent with the picture of an expanding fireball and

its dissociation at the freeze out density. Therefore, if coalescence is still working for data on a wide kinematic range, it will be interesting to determine the size of the fireballs from the new p_0 values and study its dependence as a function of incident energy and target-projectile combination.

An interesting feature of these thermal models (9,10) is also to relate the proton "freeze out" or "break-up" density to the ratio between the number of complex fragments and protons produced

$$\frac{N_o(x,y)}{N_o(1,0)} = \frac{A^{3/2}}{2^A} z_{int} \left[\rho_p \lambda_T^3 \right]^{A-1} R^y \quad (8)$$

where ρ_p is the proton density, λ_T is the thermal wavelength for protons :

$$\lambda_T = h/(2\pi m T)^{1/2} \quad (9)$$

$N_o(x,y)$ is the normalization of the momentum distribution. For a non relativistic Maxwell-Boltzmann distribution for instance, we have

$$\frac{d^3N(x,y)}{dp^3} = N_o(x,y) \frac{e^{-E/T}}{(2\pi m_a T)^{3/2}} \quad (10)$$

From the analysis of the 250 MeV/A and 400 MeV/A Ne + U data, R. Bond et al. (10) found a baryon density at break-up which is .4 that of normal nuclear matter.

Finally, light fragment cross-sections have been calculated in the framework of the firestreak model (11). Up to now it is the only model able to calculate simultaneously cross-sections for pion, proton and composite particle production. The overlap region is divided into streaks. In each of them, the nuclear matter is treated as a thermodynamic system in chemical equilibrium. Fig. 10 shows that the relationship given by eq.(2) does not hold in the firestreak model, because each streak contribute to the cross-section with a different temperature. Therefore, we have investigated which of the coalescence or firestreak models reproduce the experimental data.

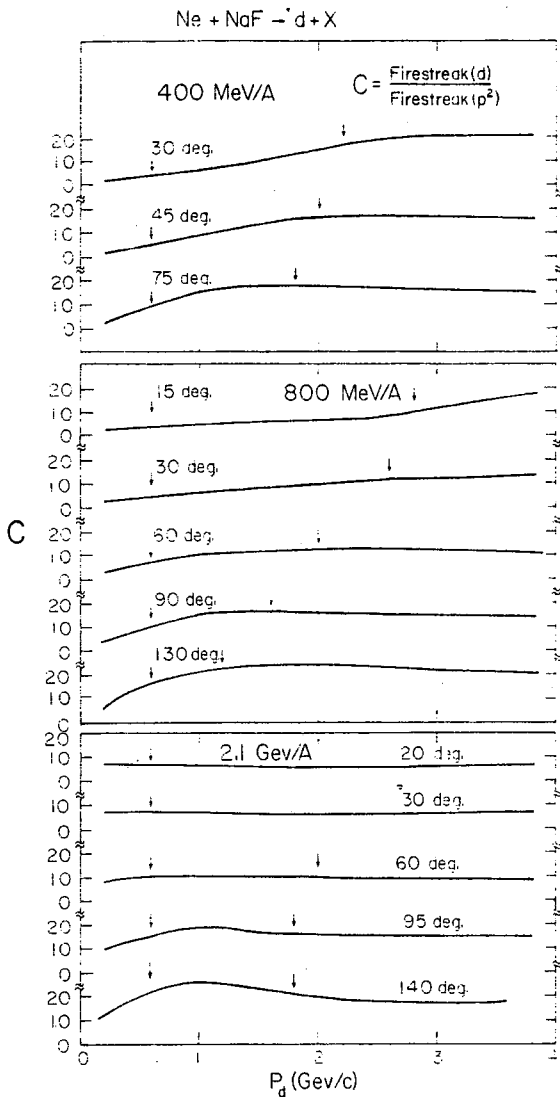


Fig. 10 - Ratio C of the deuteron cross-section to the square of the proton cross-section calculated at the same momentum per nucleon in the framework of the firestreak model.

C. Discussion

Fig. 11 to 19 display comparisons of the inclusive data with the predictions of the coalescence and firestreak models. For all the systems studied at different incident energies, the shapes and relative yields of the momentum spectra are much better reproduced with the coalescence model than with the firestreak model.

The coefficients C , p_0 and \tilde{p}_0 derived from the analysis of the experimental data with the coalescence model are listed in Table 2; p_0 and \tilde{p}_0 appear to be independent of incident energy, decrease as the sizes of the target-projectile combinations increase. \tilde{p}_0 is systematically smaller for deuterons than for tritons and ^3He . For Ne on Pb system, the volumes are a factor 4 smaller than those previously

reported for the Ne on U system. The radius R of the equivalent sphere ($V = \frac{4}{3} \pi R^3$) can be empirically expressed by :

$$R = a(A_p^{1/3} + A_T^{1/3}) + b \quad (11)$$

with $a = 0.24 \pm 0.08$ fm, $b = 1.9 \pm 0.5$ fm for deuterons and $b = 1.5 \pm 0.5$ fm for tritons and ^3He .

The deviation from a Maxwell-Boltzmann distribution has been clearly observed in the 90° c.m. deuteron spectrum measured at 400 MeV/A for the Ne + NaF system. Such flattening of the distribution at low momenta has also been seen in the proton distributions at 400 and 800 MeV/A incident energy and has been

Table 2

C, p_0 , \tilde{p}_0 , and R derived from the present data. Typical experimental errors are $\pm 30\%$ for C and $\pm 10\%$ for p_0 , \tilde{p}_0 , and R. Unit of C is $(\text{mb}/\text{sr}/(\text{GeV})^2)^{1-A}$.

a), b) Proton inclusive spectra measured in two sets of runs a) and b) differ by at most 30%, which is within the range of precision expected on the determination of absolute cross-sections. Therefore it introduces errors on C, p_0 , \tilde{p}_0 , and R which are still smaller than those quoted above.

system	energy MeV/A	σ_0 mb	fragment	C	p_0 MeV/c	\tilde{p}_0 MeV/c	R fm	
C + C	800	939	d	3.33×10^{-5}	304	167	2.9	
			t, ^3He	6×10^{-10}	280	204	2.6	
C + Pb	800	2964	d	6×10^{-6}	221	122	3.9	
			t	3×10^{-11}	219	159	3.4	
			^3He	2.5×10^{-11}	226	164	3.3	
Ne + NaF	400	1301	d	1.5×10^{-5}	259	142	3.4	
			t, ^3He	8×10^{-11}	223	162	3.3	
	800		d	1.5×10^{-5}	259	142	3.4	
			t, ^3He	2×10^{-10}	260	189	2.8	
	2100			d	1.5×10^{-5}	259	142	3.4
				t, ^3He	6×10^{-11}	212	154	3.5
Ne + Pb	400	3497	d	4×10^{-5}	205	113	4.2	
			t	1.5×10^{-11}	207	150	3.6	
			^3He	8×10^{-12}	198	144	3.7	
	800			d	4×10^{-6}	205	113	4.2
				t	1.25×10^{-11}	199	145	3.7
				^3He	5×10^{-12}	189	137	3.9
	2100			d	4×10^{-6a}	205	113	4.2
				t	2.4×10^{-6b}	173	95	5.0
				^3He	9×10^{-12}	190	138	3.9
Ar + KCl	800	2445	d	8×10^{-6a}	260	143	3.3	
			t	6×10^{-6b}	236	130	3.7	
			^3He	5×10^{-11a}	254	185	2.9	
	800			t, ^3He	3.33×10^{-11b}	238	173	3.1
				d	4×10^{-6a}	223	123	3.9
				t	3×10^{-6b}	203	112	4.3
Ar + Pb	800	4545	d	10^{-11a}	211	153	3.5	
			t	7×10^{-12b}	199	144	3.7	
			^3He	8×10^{-12a}	216	157	3.4	
			t	5×10^{-12b}	200	145	3.7	
			^3He					

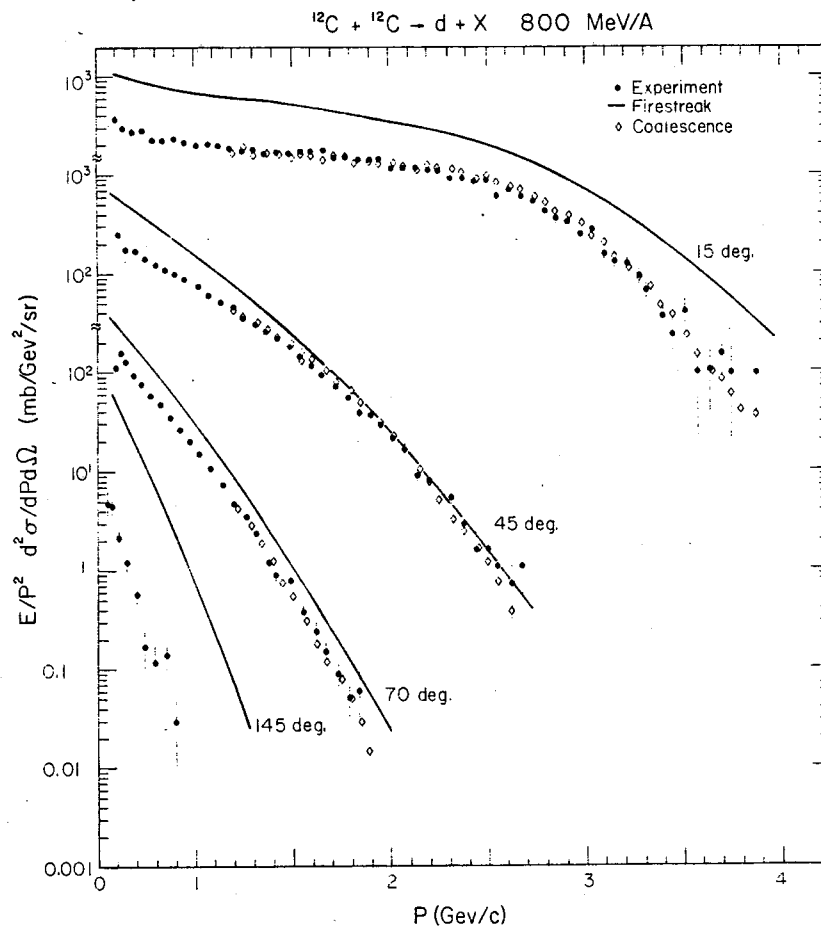


Fig. 11 - Comparison of experimental spectra for inclusive events with the predictions of coalescence and firestreak models.

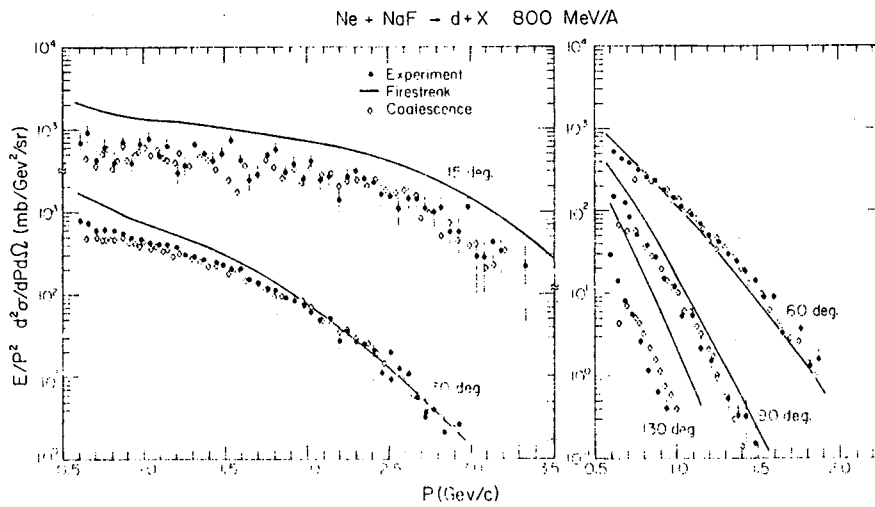


Fig. 12 - Same caption as Fig. 11.

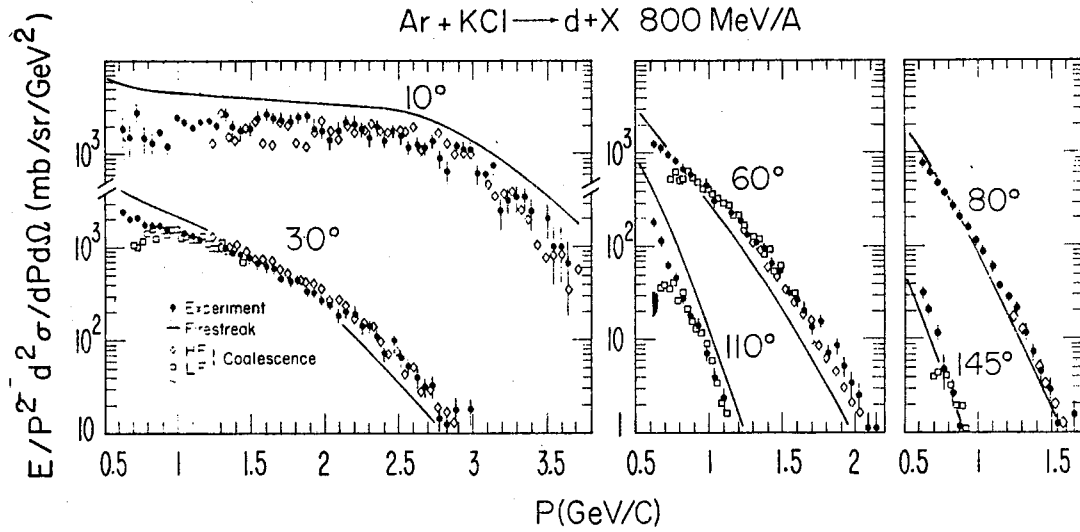


Fig. 13 - Same caption as Fig. 11.

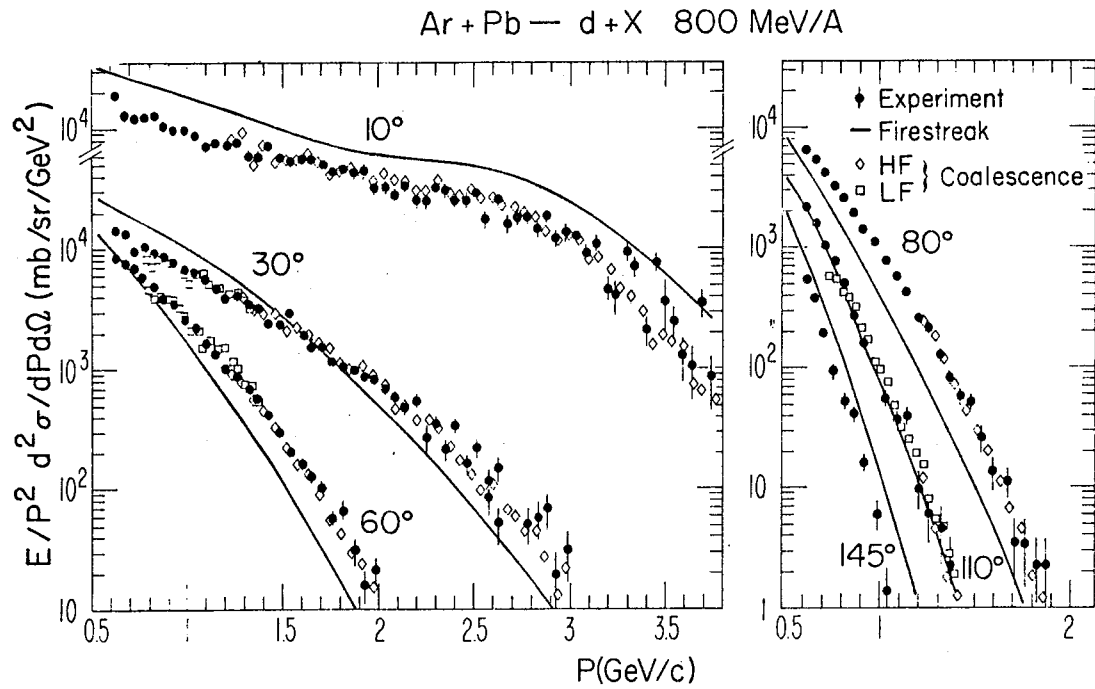


Fig. 14 - Same caption as Fig. 11.

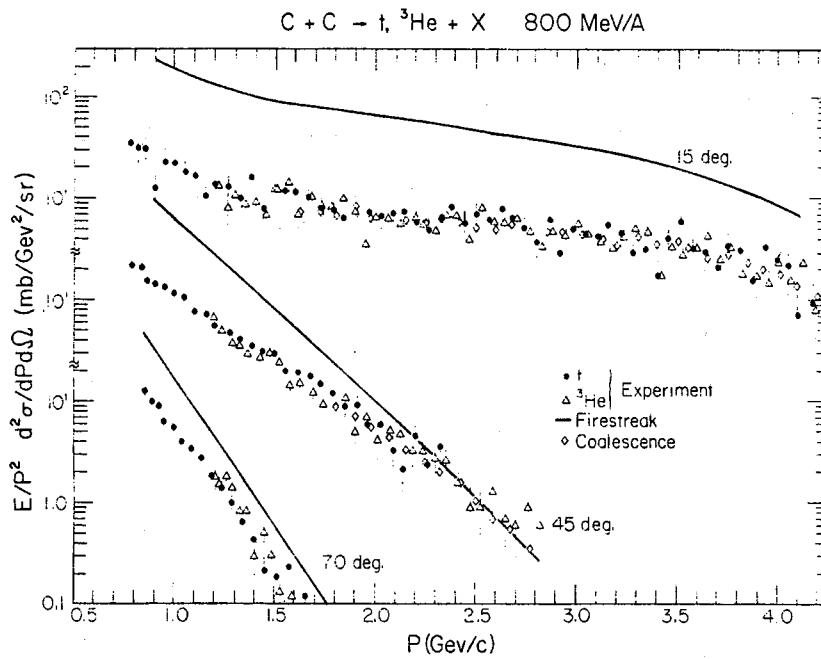


Fig. 15 - Same caption as Fig. 11.

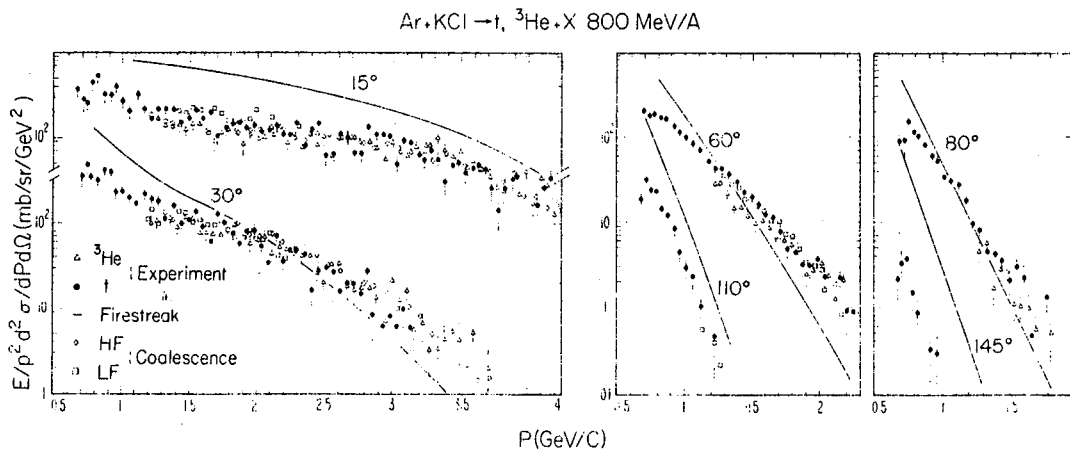


Fig. 16 - Same caption as Fig. 11.

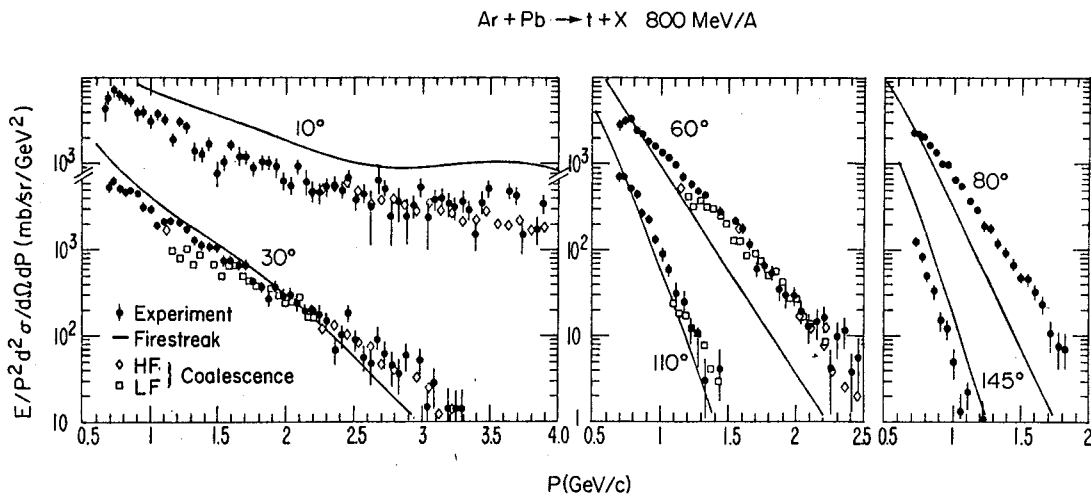


Fig. 17 - Same caption as Fig. 11.

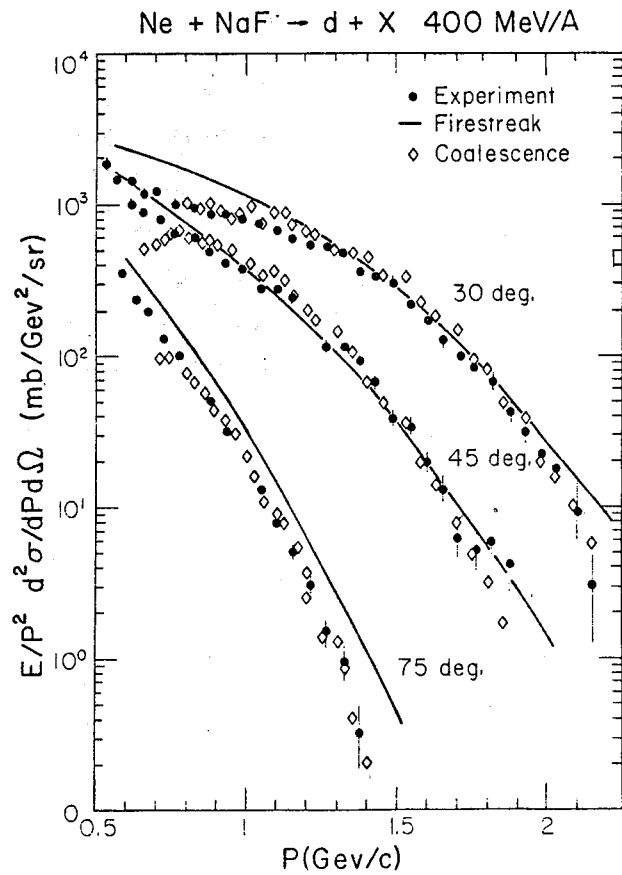


Fig. 18 - Same caption as Fig. 11.

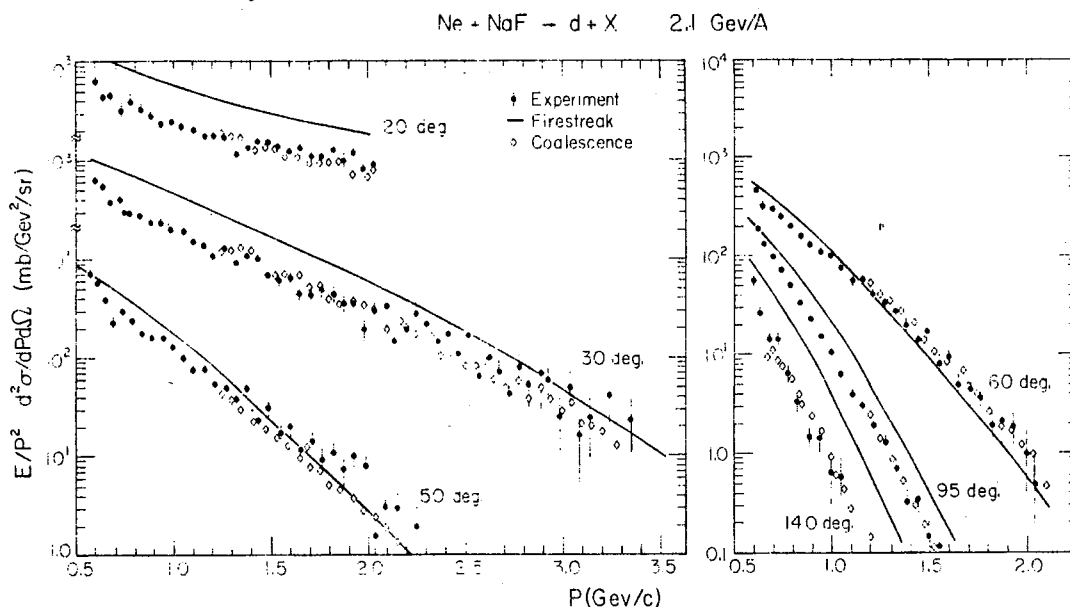


Fig. 19 - Same caption as Fig. 11.

well reproduced by the explosion model of Siemens and Rasmussen (13). Using the temperatures of fireballs and velocities for the blast wave determined from the fits to the proton and pion spectra, the 90°c.m. deuteron spectra have also been very well described by this model (13a). From the ratio of deuteron to protons, Siemens and Kapusta (13a) determined the entropy of the fireball. The result is much higher than what is expected from a soft equation of state, suggesting that either strong attractive forces are present in hot, dense nuclear matter or that degrees of freedom beyond the nucleon and pion may already be realized at an excitation energy of 100 MeV per baryon.

Finally, Fig. 20 shows that the coalescence model is also very good in reproducing the composite particle spectra once an high multiplicity selection has been performed.

Further theoretical work is required to describe the composite fragment production as none of these models have yet taken into account effects like the complex fragment size, the fireball lifetime. In addition, these models are generally valid only for one impact parameter, while the data result to impact parameter averaging. Therefore, it is interesting to compare the fireball sizes determined from the present analysis to those derived from the pion data.

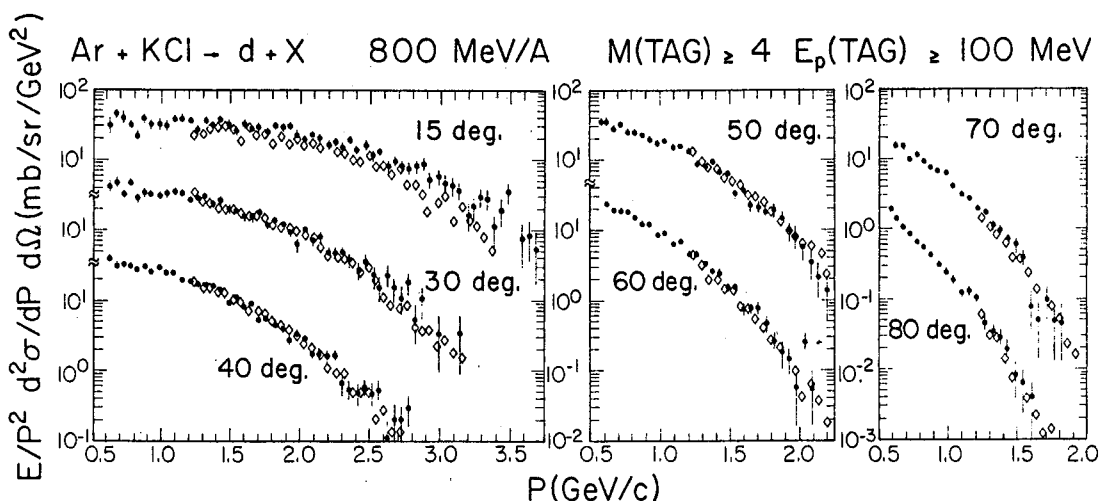


Fig. 20 - Comparison of experimental spectra for high multiplicity events with the predictions of coalescence and firestreak models.

II. DERIVATION OF THE SOURCE SIZE FROM PION INTERFEROMETRY EXPERIMENTS

In the past few years, the determination of the source size from the measurement of the Hanbury-Brown-Twiss effect (14) has been suggested by several theorists (15,16). The principle for deriving such source size from two pion correlation data can be explained in the following oversimplified way (17,18) : consider two pions emitted at the same momentum (within Δp) and at the same time (within Δt) from the points 1 and 2 of the overlap region, there are two indistinguishable ways of observing a coincidence in two detectors located at points A and B : (1 → A, 2 → B) and (2 → A, 1 → B). The two corresponding amplitudes will interfere when the uncertainty principle $\Delta p c \Delta t \leq \hbar$ is satisfied. Then, the two particle cross-section is an expression like :

$$\sigma(A+B) \propto |\phi(1 \rightarrow A ; 2 \rightarrow B) + \phi(1 \rightarrow B ; 2 \rightarrow A)|^2 \quad (12)$$

$$\propto 1 + \cos(k R \theta) \quad (13)$$

where R is the distance between the two point sources 1 and 2, $k = p/\hbar$.

Therefore, the interference term allows to determine the separation distance R of the pions at the momentum of their production. For a realistic calculation one has to integrate over all possible source points. Analytic expressions have been derived for this interference term (also called correlation function) assuming different distributions of the source points. For a gaussian space-time distribution, Yano and Koonin (16) have derived a correla-

tion function with the following form :

$$C(q, q_0) = \exp \left[- \left(\frac{\tau^2 q_0^2}{2} \right) - \left(\frac{r_0^2 q^2}{2} \right) \right] \quad (14)$$

where q is the relative momentum between the two pions, $q = |\vec{p}_1 - \vec{p}_2|$ and q_0 is the energy difference, $q_0 = |E_1 - E_2|$, r_0 and τ are respectively the radius and lifetime of the source. Assuming a uniform distribution of the source points, Kopylov (19) shows that the correlation function has the following form :

$$C(q, q_0) = \frac{I^2(r_0 q / \sqrt{2})}{1 + (\tau q_0)^2} \quad (15)$$

with $I(x) = 2 J_1(x)/x$ where J_1 is the Bessel function of the first kind.

The first measurement of pion interferometry has been carried out by Fung et al. (20) using a streamer chamber. They measured a two pion correlation function defined as :

$$R(\vec{p}_1, q) = \sigma_0 \frac{d^2\sigma}{d\vec{p}_1 d\vec{p}_2} / \left(\frac{d\sigma}{d\vec{p}_1} \right) \left(\frac{d\sigma}{d\vec{p}_2} \right) = K \left[1 + C(q, q_0) \right] \quad (16)$$

where $d^2\sigma/d\vec{p}_1 d\vec{p}_2$ is the two pion exclusive cross-section and K is an arbitrary normalization constant. The experimental data are displayed on Fig. 21. They have been taken with an 1.8 GeV/nucleon Ar beam. Fig. 21a and 21b show the data respectively for $B_a I_2$ and $Pb_3 O_4$ targets and an inelastic trigger mode which just eliminates 10 to 15 % of the most peripheral events. Fig. 21c exhibits the $Pb_3 O_4$ data for a trigger which selects central collisions. Equivalent good fits to the experimental data were obtained with a gaussian or an uniform distribution of the source points. The values of r_0 and τ are also quite independent of the distribution chosen (Table 3).

For a $Pb_3 O_4$ target, the values of $r_0 = 3.3 \mp .9$ fm and $3.98 \mp .78$ fm obtained respectively with an inelastic and a central trigger mode are in fairly good agreement with the values of 3.4 to 4.3 fm obtained from the analysis of the complex fragment emission. Recently, Bartke et al. (21) also reported a radius of 3.3 ± 0.6 fm for the C + Ta system at 3.4 GeV/A.

Further pion interferometry measurements are required to study the target projectile and energy dependence of the source sizes determined by this method.

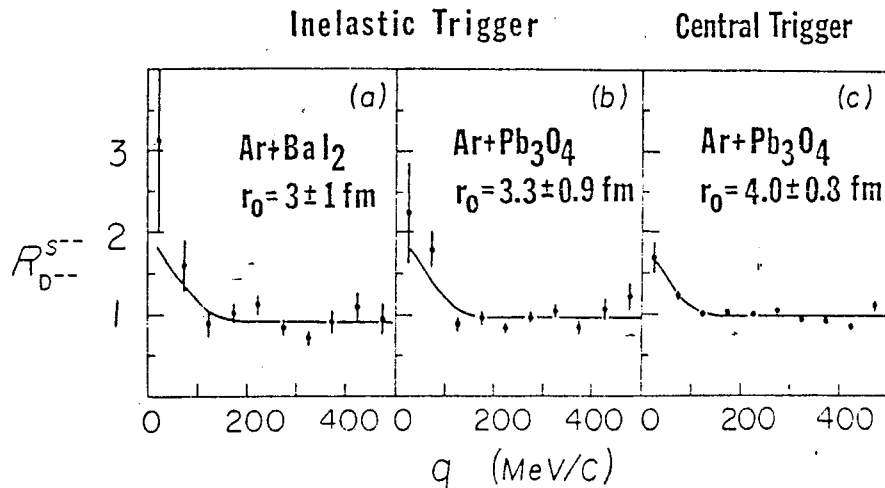


Fig. 21 - Ratio R defined by eq. (15) as a function of relative pion momentum q 1.8 GeV/nucleon ^{40}Ar beam incident on (a) BaI_2 and (b) Pb_3O_4 in an "inelastic" triggering mode, and on (c) Pb_3O_4 triggering on the most central collisions (20).

Table 3

Target	eq. (13)		eq. (14)	
	r_0 (fm)	τ (10^{-24} sec)	r_0 (fm)	τ (10^{-24} sec)
(a) BaI_2	3.05 ± 1.10	5	3.09 ± 1.17	5
(b) Pb_3O_4	3.3 ± 9.3	5	$2.98 \pm .76$	5
(c) Pb_3O_4	$3.98 \pm .78$	$2.0 \begin{smallmatrix} + 4.0 \\ - 1.8 \end{smallmatrix}$	$3.88 \pm .64$	$3.2 \begin{smallmatrix} + 4.6 \\ - 2.0 \end{smallmatrix}$

It would also be interesting to measure the correlation function C in the region of small (q, q_0) as the reduction from 1 will provide some information about the degree of coherence of the pion source (15). Such coherent effects could appear if a condensed pion field could be present in the hot zone. Theoretical work (22) is presently in progress to study the influence of Coulomb effects between the two pions, or between the pion and the nuclear matter around, the influence of rescattering and absorption effects on the determination of r_0 , τ and the degree of coherence.

III. DISTRIBUTION OF CHARGED PARTICLES ASSOCIATED WITH THE EMISSION OF A COMPLEX FRAGMENT

The distribution of charged particles associated with the detection of a complex fragment has been studied by the Poskanzer-Gutbrod group (4). The detection of fragments ranging from beryllium to fission-like events was performed with a telescope having an ionization chamber as ΔE element. Using this telescope as a trigger, they measured the associated charge particle multiplicity with eighty scintillators arranged around the scattering chamber in four angular domains : ring A from 9–20°, ring B from 20 to 45°, ring C for 45 to 80° and finally ring D at back angles (Fig. 22).

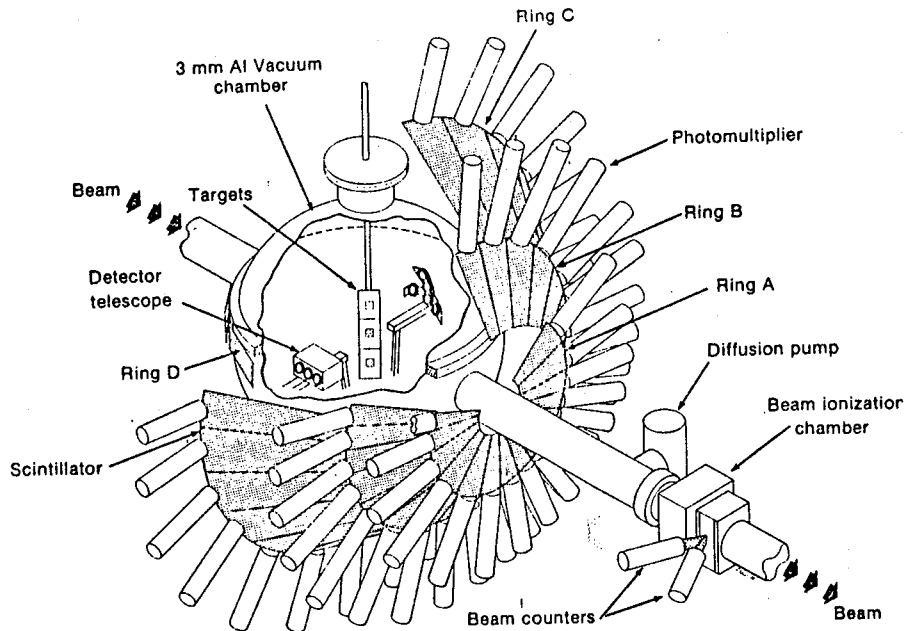


Fig. 22 - Sketch of the detector system employed by the LBL-GSI-Marburg group (4).

For the Ne on Au system studied at 400 MeV/A incident energy, Fig. 23 shows a comparison of the associated multiplicity distribution when a slow heavy fragment is detected to those observed when protons are used as a trigger. The emission of a fragment like 0 selects a central collision, while the detection of fragment with $Z > 26$ again fills up the low multiplicity region. This low multiplicity component associated with the detection of an heavy fragment has been identified as due to fission events as in case of U target where the fission cross-section is known to be large, just this component is observed.

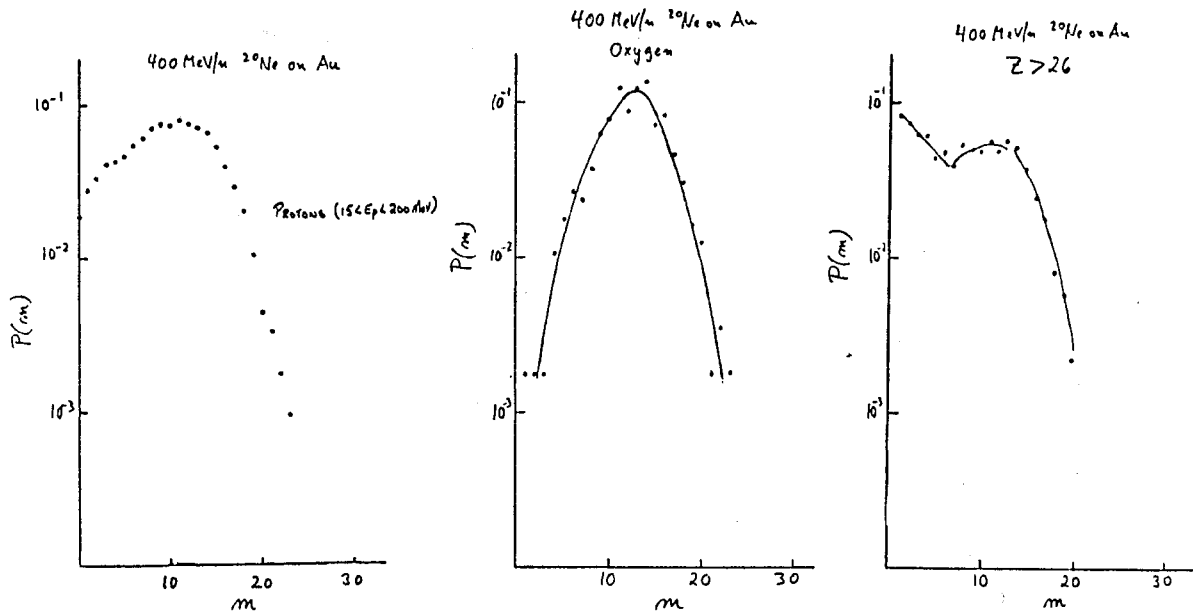


Fig. 23 - Histograms of the " m fold" coincidences associated with the detection of different fragments in the collision of 400 MeV/A Ne on Au.

Finally, on Fig. 24 are displayed the ϕ correlation obtained by detecting an heavy fragment at 90° and looking at the azimuthal distribution of the fast

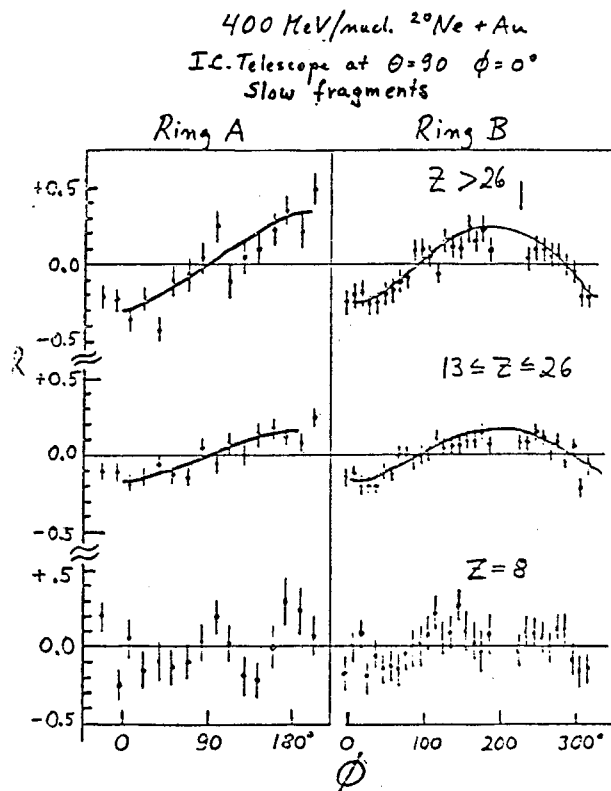


Fig. 24 - Azimuthal distribution of the fast charged particles associated with the detection of an heavy fragment.

charged particles. In case of 0 the response is very flat as expected for central events. In contrast, an enhancement at 180° appears when an heavier fragment is detected as a trigger. Such side-kick may correspond to the prediction of the hydrodynamical model (23), in which for intermediate impact parameters the beam comes in, kicks the heavy fragment off to the side while a shower of light fragments goes out oppositely.

IV. SUMMARY AND POSSIBLE FUTURE DIRECTIONS

It has been shown that the coalescence model describes very well the inclusive data for all target projectile combinations and with a coalescence radius p_0 which is independent of incident beam energy between 400 MeV and 2.1 GeV per nucleon. One may extend such study at lower incident energies as deviations from this model have been reported for data taken with a 180 MeV/nucleon α projectile (24). From the 800 MeV/A Ar beam data, it seems that the coalescence model still reproduces the experimental spectra of composite fragments when an high multiplicity selection is performed. It will be interesting to investigate further such observation in case of different target-projectile combinations and for different incident energies. Indeed, it is for central collisions that a thermal equilibrium is most likely to be reached. However, it has been recently shown (25) that the impact parameter averaging introduces the value of the two particle correlation function in the expression of the coefficient C of the usual power law relationship. Therefore, the determination of p_0 or the "break-up" density requires the measurement of this two particle correlation function in addition to the measurement of the deuteron spectra.

The study of multiparticle correlations with multiplicity selection are also of particular interest and 4π detectors are well suited for such experiments. It has already been discussed how two pion correlation experiments allow to determine the size of the fireball and the degree of coherence of the pion field. Another interesting task will be to look for a collective flow as predicted by hydrodynamical calculations (23-26). No evidence of such collective flow has been seen from the inclusive spectra partly because the averaging over various impact parameters smears out the effect while structures in the angular distributions are expected for events corresponding to truly central collisions. Criteria to select such events have been suggested by Bertsch and Amsden (27) for the collisions of two equal nuclei and by C.Y. Wong (28) for the collision of both equal and non equal nuclei. For instance, the total c.m. kinetic energy in the longitudinal direction can be used to characterize the impact parameter (26). They also show how to measure the degree of departure from azimuthal symmetry from the angular distribution of the reaction products.

Finally, one may determine the number of participants in the fireball from

two body rapidity correlations. Indeed, in high energy p-p collisions (29), the measurement of rapidity correlation function for different multiplicity selections provide some evidence for the existence of short range correlations as the detection of a particle at a given pseudo-rapidity favors the production of other particles at the same pseudo-rapidity. The interpretation of such data in terms of the cluster model shows that the peak height is related to the multiplicity of particles inside the cluster (or the fireball). In heavy ion collisions such short range correlations are expected between particles of a fireball or a streak. As in high energy data, multiplicity selection will be necessary to see such short range correlations because the number of participants of the fireball depends on impact parameter.

ACKNOWLEDGMENTS

The author would like to thank particularly O. Chamberlain, S. Nagamiya, S. Schnetzer, G. Shapiro, H. Steiner and I. Tanihata for their fruitful collaboration in the work on composite fragment production presently discussed. J. Gosset and J. Hufner are also gratefully acknowledged for having strongly stimulated this work.

This paper was supported in part by the Nuclear Science Division of the U. S. Department of Energy under contract number W-7405-ENG-48.

REFERENCES

- (1) S. Nagamiya, Talk delivered at the present conference.
- (2) S. Nagamiya et al., J. Phys. Soc. Japan 44, suppl. (1978) 378 ;
Proc. 4th High energy heavy ion summer study, Berkeley, 1978, LBL-7766,
p. 71 ; Talk delivered at the Symposium on heavy-ion physics from 10 to
200 MeV/AMU, BNL, 1979, LBL-9494.
- (3) M.-C. Lemaire et al., Phys. Lett. 85B (1979) 38.
- (4) H. Gutbrod, Proc. 4th high energy heavy ion summer study, Berkeley,
1978, LBL-7766, p. 1.
- (5) H. Gutbrod et al., Phys. Rev. Lett. 37 (1976) 667.
- (6) J. Gosset et al., Phys. Rev. C16 (1977) 629.
- (7) L. Anderson, Ph. D. Thesis, LBL-6767 (1977).
- (8) Meng Ta-Chung and E. Moeller, Phys. Rev. Lett. 41 (1978) 1352.
- (9) A. Mekjian, Phys. Rev. Lett. 38 (1978) 640 ; Phys. Rev. C17 (1978) 1051 ;
Nucl. Phys. A312 (1978) 491.
- (10) R. Bond et al., Phys. Lett. 71B (1977) 43.
- (11) J. Gosset et al., Phys. Rev. C18 (1978) 844.
- (12) A.M. Poskanzer, invited paper for the International Conference on the
dynamical properties of heavy ion reaction, Johannesburg, August 1978.
- (13) P.J. Siemens and J.O. Rasmussen, Phys. Rev. Lett. 42 (1979) 880.
- (13a) P.J. Siemens and J. Kapusta, Preprint.
- (14) R. Hanbury-Brown and R.Q. Twiss, Nature 178 (1956) 1046.
- (15) M. Gyulassy, LBL-7704 (1978).
- (16) F.B. Yano and S.E. Koonin, Phys. Lett. 78B (1978) 556.
- (17) G. Cocconi, Phys. Lett. 49B (1974) 459.
- (18) B. Schürman, Notes of lectures delivered at INSTN, December-January 1978/
1979.
- (19) G.I. Kopylov, Phys. Lett. 50B (1974) 472.
- (20) S.Y. Fung et al., Phys. Rev. Lett. 41 (1978) 1592.
- (21) J. Bartke et al., Contributed paper 6D18 to the Vancouver Conference,
August 1979.
- (22) M. Gyulassy, S.K. Kauffman and L.W. Wilson, LBL-8750.
- (23) J.R. Nix, Proceedings of the symposium on relativistic heavy ion research
GSI Darmstadt (1978) vol.2, p.317.
- (24) Doering et al., Phys. Rev. Lett. 40 (1978) 1433.

- (25) J.I. Kapusta, LBL-9251.
- (26) H. Tang and C.Y. Wong, to be published.
- (27) G. Bertsch and A.A. Amsden, Phys. Rev. C18 (1978) 1293.
- (28) C.Y. Wong, preprint.
- (29) L. Foa, Phys. Rep. 22C (1975) 1.

